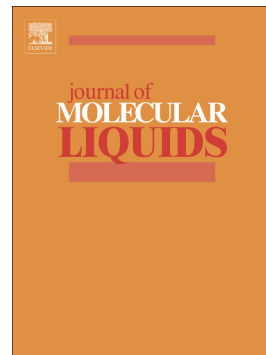


Accepted Manuscript

Facile green fabrication of nanostructural Ni-doped ZnO hollow sphere as an advanced photocatalytic material for dye degradation

Seyed Mohsen Mousavi, Ali Reza Mahjoub, Reza Abazari



PII: S0167-7322(17)31525-8
DOI: doi: [10.1016/j.molliq.2017.07.050](https://doi.org/10.1016/j.molliq.2017.07.050)
Reference: MOLLIQ 7628

To appear in: *Journal of Molecular Liquids*

Received date: 8 April 2017
Revised date: 9 July 2017
Accepted date: 14 July 2017

Please cite this article as: Seyed Mohsen Mousavi, Ali Reza Mahjoub, Reza Abazari , Facile green fabrication of nanostructural Ni-doped ZnO hollow sphere as an advanced photocatalytic material for dye degradation, *Journal of Molecular Liquids* (2017), doi: [10.1016/j.molliq.2017.07.050](https://doi.org/10.1016/j.molliq.2017.07.050)

This is a PDF file of an unedited manuscript that has been accepted for publication. As a service to our customers we are providing this early version of the manuscript. The manuscript will undergo copyediting, typesetting, and review of the resulting proof before it is published in its final form. Please note that during the production process errors may be discovered which could affect the content, and all legal disclaimers that apply to the journal pertain.

Facile green fabrication of nanostructural Ni-doped ZnO hollow sphere as an advanced photocatalytic material for dye degradation

Seyed Mohsen Mousavi ^{a,b}, Ali Reza Mahjoub ^{a,*}, Reza Abazari ^a

^a Department of Chemistry, Tarbiat Modares University, P.O. Box. 14155-4383 Tehran, Iran

^b Assistant Professor, Department of Chemistry, Farhangian University, Tehran, Iran

E-mail: mahjouba@modares.ac.ir; smm4566@gmail.com; reza.abazari@modares.ac.ir; Fax:

+98 21 82883455; Tel.: +98 21 82883442.

Abstract

Through a green protocol, hollow forms of x -Ni-ZnO ($x = 0, 2, 3, 5,$ and 10 wt % Ni) were prepared in ultrasonic bath at a low temperature using template fructose. For characterizing the shape, structure, crystallite phase, purity, and chemical composition of the prepared hollow spheres, the powder X-ray diffraction (PXRD), fourier transform infra-red spectroscopy (FT-IR), field-emission scanning electron microscopy (FE-SEM), energy dispersive analysis of X-ray (EDAX), High-resolution transmission electron microscopy (HRTEM), inductively coupled plasma (ICP), and ultraviolet-visible absorption (UV-Vis) spectroscopy were employed. Besides, the photo-catalytic properties of these hollow spheres for degrading Congo Red (CR) as an Azo dye were taken into account. According to the results, Ni-ZnO hollow spheres outperform the pure ZnO hollow spheres in terms of the photocatalytic activities. Furthermore, in order to show the impact of various morphologies on the CR dye degradation, the Ni-ZnO nanostructures were produced with rod-like, flower-like, and wood-like morphologies. Our synthesized Ni-ZnO hollow spheres seem to be highly promising for future applications in different commercial fields and industries. Moreover, they are applicable for photodegradation of other organic pollutants.

Keywords: X-Ni-ZnO, Hollow sphere, Chemical method, Photocatalytic activity; Waste water, Azo dye.

1. Introduction

Nowadays, environment is becoming more and more contaminated by the emission of different dye pollutants from the industries. In spite of the fact that different chemical and biological degradation methods have already been proposed to remove such dye pollutants from wastewater, the results have shown to be largely unsatisfactory [1-3]. In recent years, application of semiconductors (e.g., ZnO and TiO₂) for the photocatalytic degradation of the dye pollutants in water has received much attention since these photocatalysts are highly efficient, inexpensive, ecofriendly, and nonpoisonous [4–7]. However, since ZnO and TiO₂ show a low solar energy conversion efficiency, have a wide band gap of 3 to 3.2 eV, and demonstrate a high charge recombination rate of the photo-induced electron/hole pairs, their applications in the semiconductor photocatalytic oxidation for removal of the environmental contaminants is restricted [8-11]. Furthermore, TiO₂ and ZnO react only towards the UV illumination which is less than 4 percent of the solar spectrum, their photo-catalytic yields and practical uses are limited [12]. Consequently, a substantial challenge is to develop innovative photocatalysts with superior stability and efficient visible light absorption [13-16]. As recorded in the literature, ZnO has a more appropriate photocatalytic efficiency than TiO₂, which can be explained by its quite high absorption over a greater portion of the UV light spectrum. Besides, in comparison with TiO₂, ZnO is intensely luminescent and serves as a highly active photocatalyst. The quick recombination of the charge carriers is the key factor that affects the ZnO photocatalytic activities [17-19].

Some previous studies have considered the ZnO coupling with other semiconductors. The reasons for this are to improve the light adsorption and light utilization efficiency and to increase the separation of the photogenerated electrons and holes [20, 21]. Therefore, various ions are

able to be doped into ZnO so that the recombination of the photo-generated pairs of electron-hole can be inhibited. From the literature, Ni²⁺ ion is known to be a crucial dopant related to the magnetic materials [22, 23]. Moreover, Ni²⁺ can be substituted for Zn²⁺ in ZnO lattice due to the fact that Ni²⁺ (0.69 Å) has a valence which is identical to that of Zn²⁺ and has a radius which is close to that of the Zn²⁺ (0.74 Å). In their study, Zhu and his colleagues concluded that Ni-doping is likely to improve the photocatalytic oxidation of aromatic alcohols in NH₂-MIL-125(Ti) [24]. Sasikala et al. suggested a route for enhancing the photocatalytic efficiency of the Ni doped CdS nanostructures [25].

As proposed in the literature, preparation of the metal oxide nanostructures with controllable size and morphology is of great importance for their potential applications. This can also help to control the chemical and physical features of these materials [26-28]. Some previous works have already reported the Ni-ZnO hetero-structured nano-crystals (e.g., as particle and nanowire). However, in recent years, much weight has been given by different researchers to the preparation of the nanostructural Ni-ZnO hollow spheres because the hollow spheres demonstrate a large surficial area, low density, distinct optical properties, and good permeation [29], and are easily applicable in various scopes like drug delivery, catalysis, photonic crystals, etc. A number of synthesis methods have already been introduced to produce these materials from compounds. Most of these synthetic methods have presumed the silica nanospheres to be a sacrificial template material. While silica colloids can be observed in different commercial sizes, the removal of the silica templates may take a long time and highly aggressive and toxic hydrofluoric acids are inevitably used. Thus, an urgent need can be felt for introducing a straightforward preparation route under such mild conditions as low temperature and reduced

workup. In one of our previous works, through the carbon microspheres pattern, we made use of the ZnO hollow spheres for the degradation of the Congo Red pollutant [30].

In the present study, using a facile, ecofriendly, and energy-saving sonochemical approach, preparation and characterization of the nanostructural x-Ni-ZnO (x = 0, 2, 3, 5, 10 wt % Ni) hollow spheres are for the first time prepared and characterized. Here, for the formation of the hollow core, carbon microspheres are employed as a template that can be spontaneously removed. Moreover, for investigation of the photocatalytic behavior of these hollow spheres, CR dye degradation is taken into account.

2. Experimental

2.1 Materials and physical techniques

All reagents for the synthesis and analysis were commercially available from Merck Company and used as received. Fructose, zinc(II) acetate dihydrate (Merck, 99.9%), nickel (II) acetate tetrahydrate (Merck, 99.9%). Doubly-distilled water was used to prepare aqueous solutions. The infrared spectra were recorded on a Nicolet Fourier Transform IR, Nicolet 100 spectrometer in the range 400-4000 cm^{-1} using the KBr disk technique. Powder X-ray diffraction (PXRD) measurements were performed using a Philips X'pert diffractometer with monochromated $\text{Cu-K}\alpha$ radiation ($\lambda = 1.54056 \text{ \AA}$). Also, the morphology of samples was characterized by a field emission scanning electron microscope (FE-SEM) (Mira TESCAN) with gold coating. The UV-Vis absorption spectra were examined on a UV-Visible spectrometer (Shimadzu UV 2100). High-resolution transmission electron microscopy (HRTEM) images were recorded with a Philips CM 30 instrument.

2.2. Synthesis of carbon spheres

The preparation route typically used for carbon spheres is as follows [31]. Fructose dissolving (10 grams) in deionized water (100 ml) was first performed to obtain a transparent solution. After that, the obtained suspension was transferred into a 150-ml Teflon-lined autoclave. At a temperature of 160 °C and for 4 hours, the autoclave was then placed into a blast drying oven and heated. After cooling down the oven to room temperature, through infiltration, the resultant carbon spheres were separated from the suspension and was subsequently washed three times with deionized water. Finally, it was dried at 80 °C for 2 h in a way that excessive water was evaporated.

2.3. Preparation of zinc oxide hollow spherical nanostructures

In an ultrasonic bath at ambient temperature for 1 hour, 2.2 g of zinc(II) acetate dihydrate was added to 40 ml of water and 1 g of carbon spheres as templates. The subsequently centrifuged mixture was washed with distilled water. After that, it was calcined in a furnace having a temperature of 500 °C for 6 hours so that ZnO hollow spheres could be synthesized.

2.4. Ni-doped ZnO hollow spheres preparation

In order to prepare x-Ni-ZnO (x = 2, 3, 5, and 10 wt % Ni) hollow spheres, in 40 mL of distilled water proper quantities of zinc(II) acetate dihydrate and nickel (II) acetate tetrahydrate of analytical reagent grade were combined and dissolved. Moreover, 1 g of carbon microspheres was homogeneously dispersed in 20 ml of distilled water. In the ultrasonic bath at room temperature, the templates were put for 1 h. The mixed solution was then aged for one day under ambient conditions. The subsequently centrifuged product was washed using distilled water.

After, the product was annealed from the room temperature to 500 °C at 1°C min⁻¹ rate and placed at 500 °C for 2 hours in air. Resultantly, Ni-ZnO hollow spherical nanostructures with a white to greenish white color were produced. The produced hollow spheres were finally employed as photo-catalyst to degrade the Congo Red pollutant.

2.5. Investigation of the photocatalytic reactions

In order to evaluate the photocatalytic behaviors of the doped and un-doped samples, the CR dye photo-catalytic degradation in water under visible light irradiation was measured. For the investigation of the photocatalytic properties, in an open Pyrex reaction vessel, 50 ml of the 10-ppm solution of the CR dye (as a suspension) and 25 mg of the suggested photocatalysts (i.e., the pure ZnO and x-Ni-ZnO hollow spheres) were utilized. During the photolysis, the magnetic stirring of this suspension was done. In order that the solution remained oxygen-saturated throughout the reaction, using an air pump, air was blown into the mixture. While the photocatalytic reaction was performed, the dispersions temperature was kept constant at 30 °C. The dye solution was first stirred in a dark place for 30 min. Under the visible light illumination of the suspension, at fixed intervals (starting from zero time) 3 mL of the homogenized dispersion aliquots were adopted and centrifuged at 4000 rpm for five minutes (The irradiation was done with a UV lamp (30 W, UV-C, $\lambda = 253.7$ nm, 4.89 eV, Philips (The Netherlands)) and/or a 400 W high-pressure mercury-vapor lamp (providing visible light ≥ 300 nm)). Through the measurement of the CR dye absorbance (at the wavelength of 598 nm), the reaction was thus assumed to be a function of the illumination time.

3. Result and discussion

Through the X-ray diffraction, structural factors and crystalline phases of the obtained samples were taken into account. XRD patterns related to the pure ZnO and x-Ni-ZnO hollow spheres are represented in Fig 1. The high crystallinity of the prepared samples is well indicated by their relatively sharp and intense peaks. Furthermore, according to the XRD patterns, all of the samples showed crystal structure with high intensity, which is in agreement with JCPDS database of card number 36-1451. As it can be seen in the figure, with the increase in the amount of Ni²⁺, no shift happens in the peaks related to the ZnO. This can be due to the closeness of the value of the ionic radius of Zn⁺² to that of the Ni²⁺. Besides, as the value of Ni²⁺ increases, its related peak goes up.

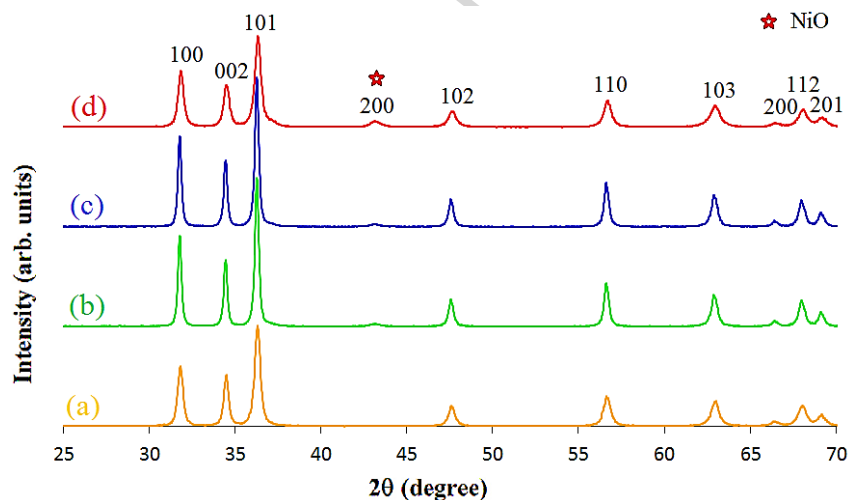


Fig. 1. XRD diffraction pattern of the x-Ni-ZnO hollow spheres [x = 0 (a), 3 (b), 5 (c), and 10 (d) wt % Ni].

FT-IR spectroscopy can afford to analyze the compound purity and characterize the structural integrity of the catalysts. Furthermore, FT-IR is highly reactive against the vibrations in the metal-oxygen bonds. In general, the region below 1000 cm⁻¹ shows that the intensive bands in

all the spectra are related to the stretching vibration mode of the M-O bond [32]. In this regard, formation of the metal oxide can be corroborated. In Fig. 2, FT-IR spectra of the pure ZnO and x-Ni-ZnO hollow spheres are represented. Therefore, the broad band at 525 cm^{-1} can be due to the stretching vibrations of $\text{ZnO}^{\text{II}}\text{-O}$. The observed band at 421.7 cm^{-1} is associated with the $\text{Ni}^{\text{II}}\text{-O}$ stretching. However, perhaps because of the slight quantity of the Ni^{II} ions in our prepared hollow spheres of Ni-ZnO, this issue cannot be observed in this figure. Furthermore, because of the adsorption of water in the produced hollow spheres, some peaks are observed at 3438 , 1631 and 1381 cm^{-1} [33, 34]. According to the Ni-ZnO hollow spheres spectra, no bands are seen for the formation of the new compound. Besides, no organic species exist while synthesizing the Ni-ZnO hollow spheres. It can thus be mentioned that FT-IR spectroscopy is in agreement with the results of the XRD patterns.

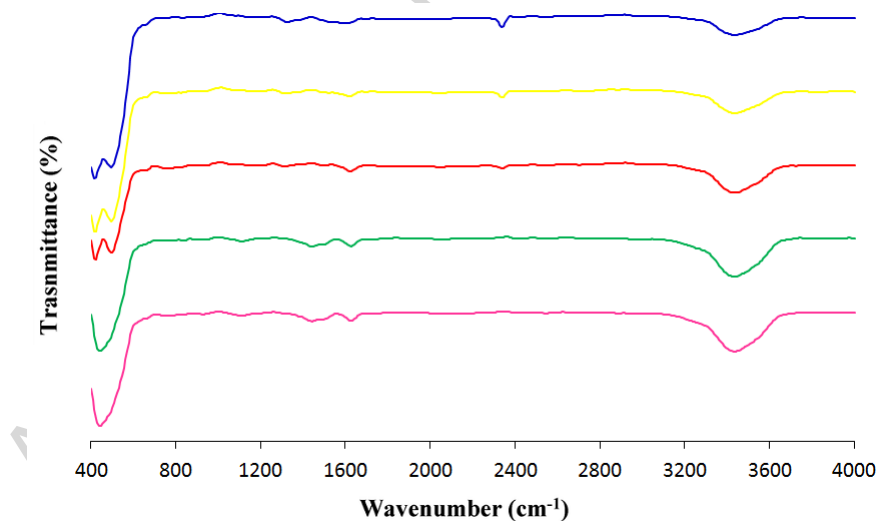


Fig. 2. FTIR spectra of the X-Ni-ZnO nanostructures [x = 0 (pink), 2 (green), 3 (red), 5 (yellow), and 10 (blue) wt % Ni].

SEM images for the surfaces of the synthesized pure carbon microspheres, pure ZnO hollow spheres, and x-Ni-ZnO hollow spheres ($x = 0, 2, 3, 5, 10$ wt % Ni) in the ultrasonic conditions are shown in Fig. 3. As Figs. 3a and 3b show, carbon microspheres have granulated and rough surfaces. The surficial granules in the present study are around 7 nm in size, which agrees with the results from the previous studies [35]. Indeed, formation of the carbon spheres surfaces is attained by the aggregation of a number of uniform carbonaceous particles that are 7 nm in size. After the calcination of carbon sphere@ZnO and carbon sphere@Ni-ZnO, pure ZnO hollow spheres and Ni-ZnO hollow spheres are obtained, which, due to the vacant space formation in their center, demonstrate a large surficial area compared to the carbon sphere@ZnO and carbon sphere@Ni-ZnO. However, due to the fact that these surficial ZnO and Ni-ZnO particles are approximately 60 nm in size, their surface area is smaller than that of the pure carbon microspheres (Figs. 3c to 3j). It should also be noted that, as it can be seen in the figures, with the increase in the amount of Ni, the particles morphology on the hollow sphere surface has changed from a state of more spherical to a state of more spiral. This can be caused by the variation in the Zn-to-Ni molar ratio, which has resulted in very slight changes in the morphology of the hollow spheres.

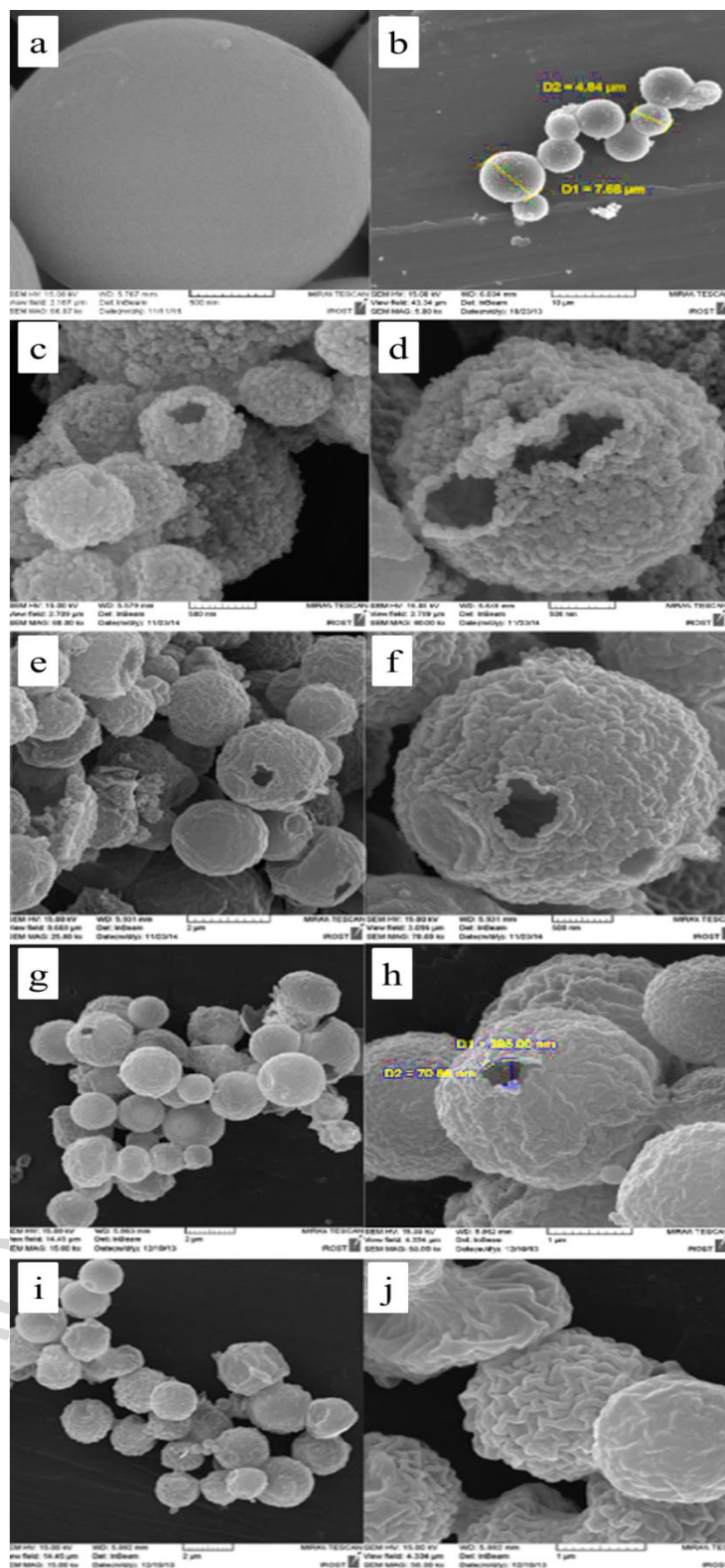


Fig. 3. SEM images of pure carbon spheres (a, b) in two different scale bars and the x-Ni-ZnO hollow spheres [x = 0 (c, d), 3 (e, f), 5 (g, h) and 10 (i, j) wt % Ni].

In order to get a better understanding of morphology of the prepared hollow spheres, HRTEM analysis is here used. HRTEM analyses of the pure ZnO hollow spheres and Ni-ZnO hollow spheres calcined at 500 °C are shown in Figs. 4a-d. The hollow spherical microstructures of the products in these images can be due to the existence of a bright internal layer and a dark external layer in the spheres. In other words, in HRTEM images, a marked difference exists between the dark edges and the light centers of the spheres. This indicates the formation of hollow spheres and is congruent with the SEM results. These layers also show sufficient overlap with enough transparency. As shown by these images, our prepared hollow spheres are 1.2-1.8 μm in diameter, while the thickness of the coarse shell is approximately 40 nm.

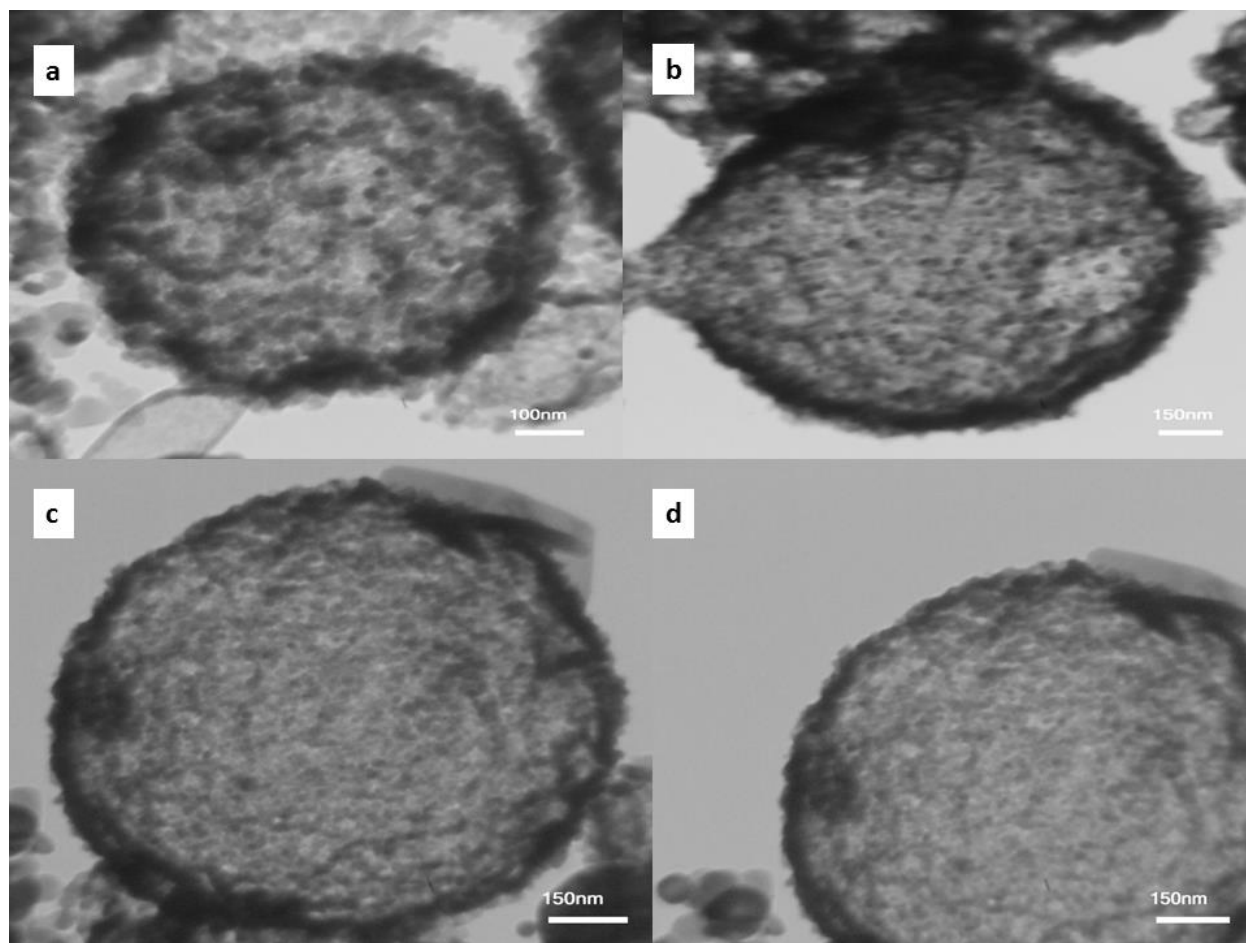


Fig. 4. HR-TEM images of the x-Ni-ZnO hollow spheres [$x = 0$ (a), 3 (b), 5 (c), and 10 (d) wt % Ni]

Besides, in this study, in order to show the presence of Ni^{2+} ions in hollow spheres, EDAX is taken into account. Fig. 5 shows the chemical composition of Ni-ZnO hollow spheres, of which the results are congruous with those of XRD patterns. The peaks shown in Fig. 5 are related to the Zn, Ni and O elements. Therefore, Ni^{2+} ions presence in these hollow spheres is confirmed. Existence of the other peaks in these spectra can be ascribed to the presence of the Au element used for the sample sputter coating at EDAX stage. Besides, as shown in the insert of the images,

the obtained weight ratios are approximately equal to the predicted value from the initial amounts during the synthesis.

Based on the EDX spectra of Ni-ZnO hollow spheres, atomic concentration of Ni²⁺ ions for Ni-doped ZnO hollow spheres is very small (2%-10%). For the Ni-doped samples, the stoichiometric ratio is comparatively appropriate. Ni ions incorporation into the ZnO lattice is also evident. A proper concord exists between the XRD and the EDX results. Also, in an effort to determine the accurate contents of x-Ni-ZnO hollow spheres, inductively coupled plasma (ICP) measurement was performed. The amounts of Ni are about 29.7, 44.7, 67.8, and 136.3 mg/L in the etching solution for the samples with 2, 3, 5, and 10 % Ni, respectively. These contents are close to the contents of raw materials, where is 28, 42, 70, and 140 mg/L, respectively. To further confirm the composition of the 3-Ni-ZnO hollow spheres as the best photocatalyst in this study, we performed elemental mapping analysis. The elemental maps of 3-Ni-ZnO hollow sphere clearly show the distribution of elements of Zn, Ni, and O in this sample (Fig. 6). As are clear from this figure, through the elemental analysis of 3-Ni-ZnO hollow spheres, it was corroborated that the Ni²⁺ ions were doped into ZnO.

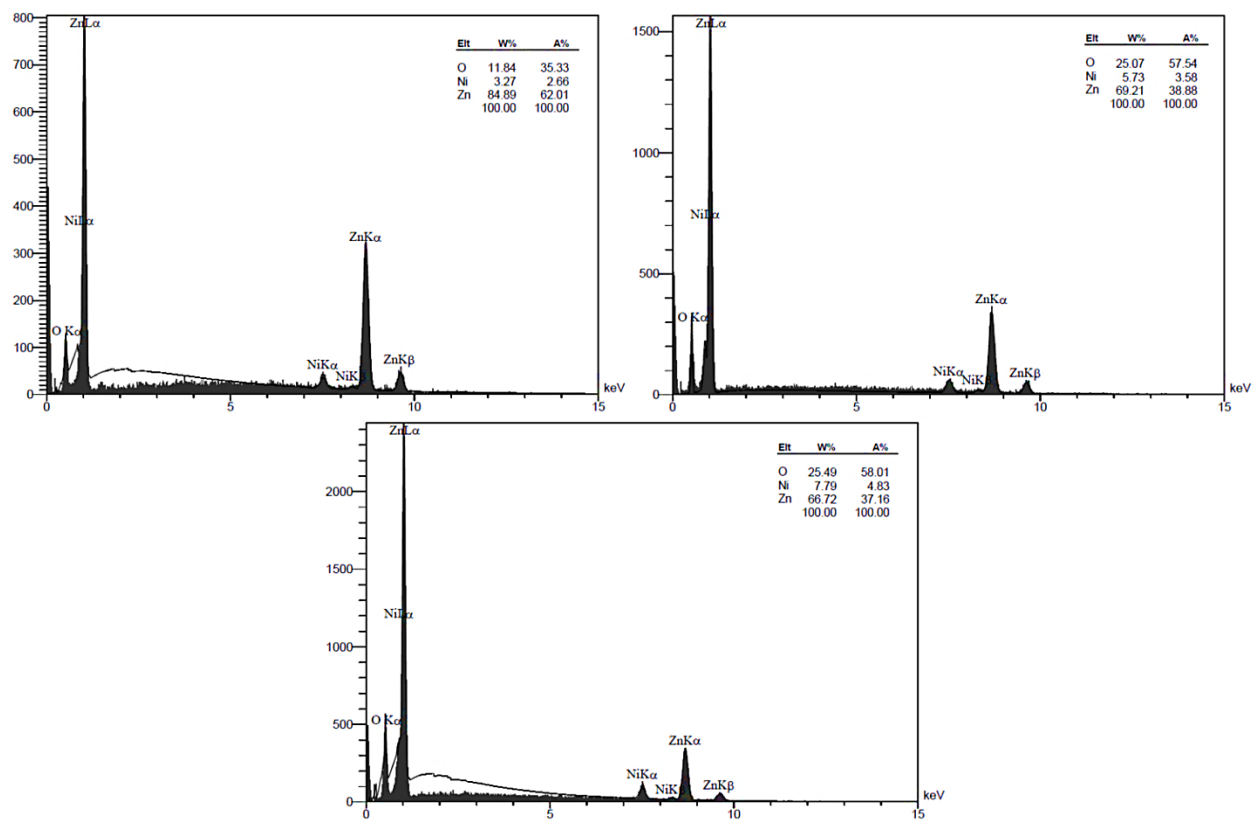


Fig. 5. EDAX analysis of the x-Ni-ZnO hollow spheres, the Ni weight content (x) is increased with the arrow [3 (a), 5 (b), and 10 (c) wt %].

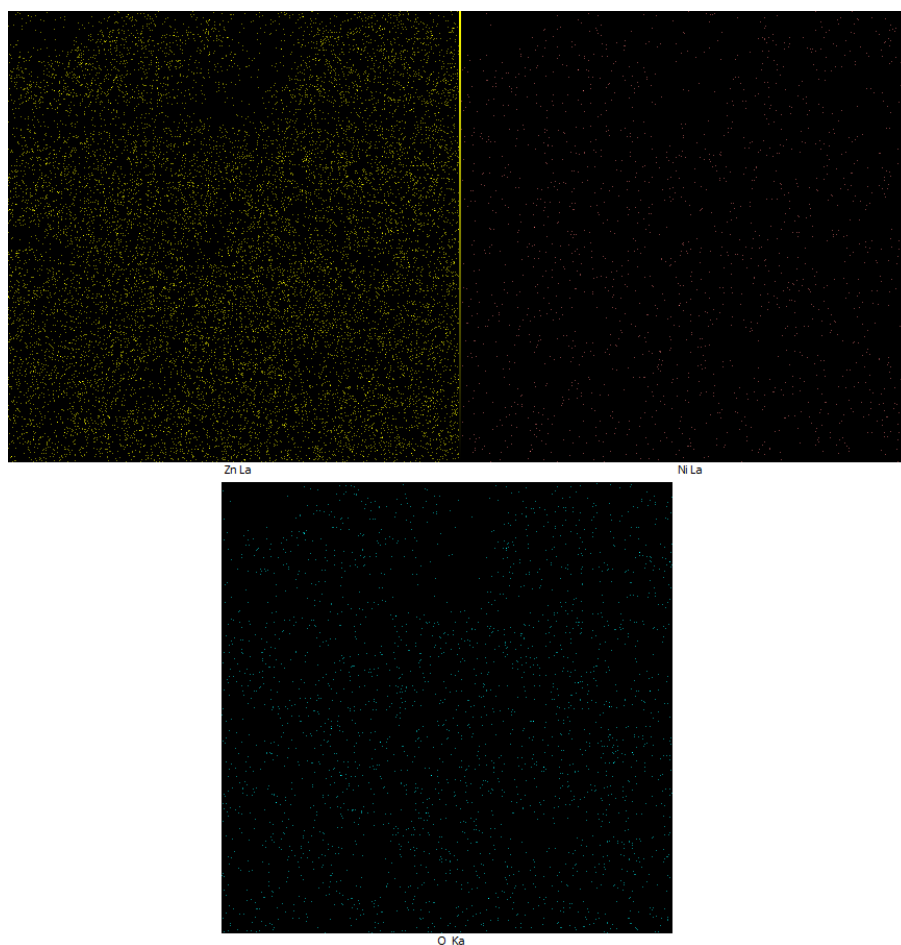


Fig. 6. The elemental mapping of the 3-Ni-ZnO hollow spheres.

In order to get a better understanding of the morphology of the prepared hollow spheres, analysis of the UV-Vis optical absorption was taken into account in order to obtain the values of the optical band gap related to the superior photo-catalytic agent of the present work (3-Ni-ZnO hollow spheres), and subsequently photocatalytic characteristics were explored. Energy band gap will be computed by relation (1). From the previous works [27], it has been found that the energy band gap and λ_{onset} are related. This can be expressed by the following formulation.

$$E_g = 1239.8 / \lambda_{\text{onset}} \quad (1)$$

In the above relation, λ shows absorption edge wavelength in nm in the spectrum and E_g stands for band gap energy (eV). Using Eq. (1), an energy band gap value of 3.02 was resulted for the prepared hollow spheres of 3-Ni-ZnO. The said value is observed to be in conformity with the reported values in the literature [37].

In Fig. 7, photocatalytic properties of the prepared hollow spheres for the CR dye photo-degradation at a pH of 9.5 are compared. In one of our previous works, we estimated the optimal value of the ZnO hollow spheres, which was equal to 9.5. Therefore, the same optimum value is also here taken into account. In the absence of light, the dye concentration does not change even in the presence of the catalyst. This well shows the importance of the light irradiation for the conduction of appropriate interactions. On the other hand, in the mere presence of light, when the synthesized hollow spheres are not used, no improvement in the photo-catalytic degradation is observed compared to the case where light irradiation was absent. The CR dye photo-catalytic degradation even after 80 min from the beginning of the reaction was unsatisfactory. In order to enhance the reaction, it is therefore required to make use of light irradiation in the presence of the catalytic quantities. In order to determine the photo-catalytic effects of the produced hollow spheres, a comparison has been made between the degradation efficiency of pure ZnO hollow spheres and x-Ni-ZnO hollow spheres. When pure ZnO hollow spheres were used as photocatalysts, the results were not good. Even after eighty minutes from the reaction beginning, the color of the solution was not transparent and a pink dye was visible to the naked eye. Using the UV-Vis, the CR dye photocatalytic degradation percentage was approximately 45%. However, the other 55% is not a negligible amount and can clearly cause a serious environmental hazard. Then, x-Ni-ZnO hollow spheres with various Ni-to-Zn weight ratios (2%, 3%, 5%, and 10%) were utilized. As Fig. 7 shows, after 80 min from the initiation of the CR dye

photodegradation, the degradation percentage for 5-Ni-ZnO hollow spheres was equal to 89%. The quantity of Ni^{2+} ions was then increased so that the x-Ni-ZnO hollow spheres quantity changed from 5-Ni-ZnO to 10-Ni-ZnO. Resultantly, a reduction in the photocatalytic efficiency was observed from 89% to 86%. In the case of 3-Ni-ZnO hollow spheres, where the quantity of the Ni^{2+} ions was reduced from 5% to 3%, the dye photocatalytic degradation was almost completed. As such, the CR dye degradation arrived at 100% after 80 min of the reaction. When the Ni^{2+} ions quantity was further reduced from 3% to 2%, the CR dye photocatalytic degradation efficiency went down and became 91%. It can thus be concluded that when the weight ratio of 3% is used for Ni to Zn (namely, 3-Ni-ZnO), the superior efficiency for these two metals is attained.

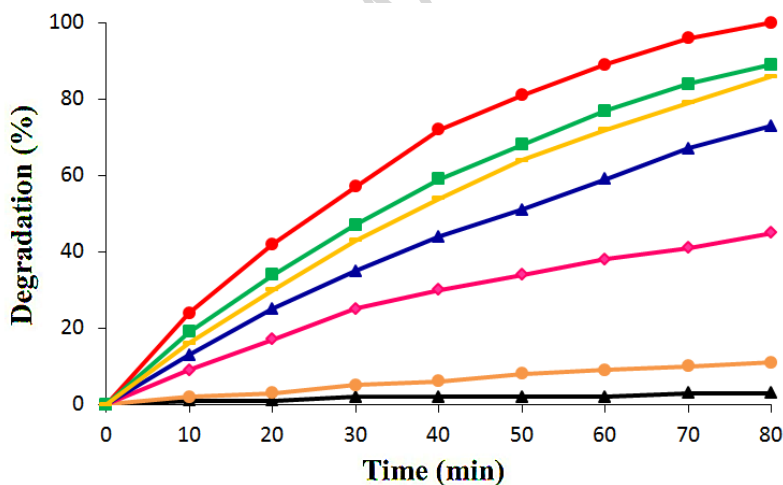


Fig. 7. Photocatalytic efficiency of the x-Ni-ZnO hollow spheres [in dark (black), without photocatalyst (orange), x = 0 (pink), 2 (green), and 3 (red), 5 (yellow), 10 (blue) wt % Ni] for CR dye degradation under ultraviolet light irradiation.

One of the advantages of the investigated photocatalyst is its stability during photodegradation reaction. Fig. 8 shows that after four repetitive usages of 3-Ni-ZnO hollow spheres each including 80 min of irradiation, no appreciable change in its photocatalytic activity occurs. So, this can be considered as a good photocatalyst for photodegradation of CR dye.

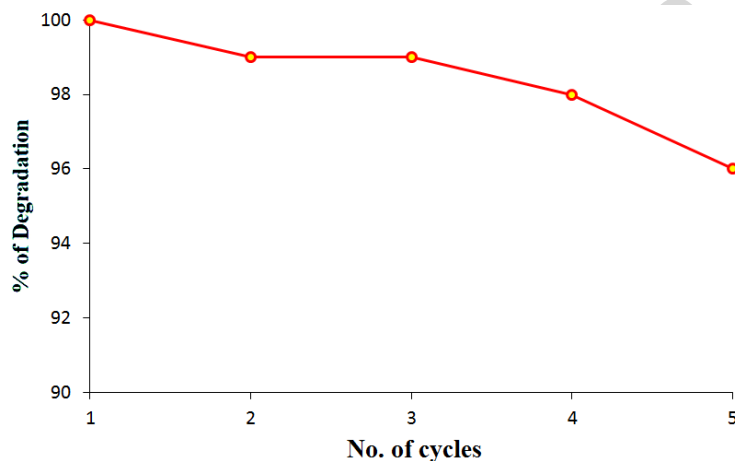


Fig. 8. Recycle and reuse of 3-Ni-ZnO hollow spheres for CR dye photocatalytic degradation.

From the literature, it is already known that nanostructural size and morphology are the key factors influencing the efficiency of the photocatalysis procedure. Therefore, in the present work, the CR dye photo-catalytic degradation has been taken into account so that the morphological impacts can be best understood. In order to explore the photocatalytic efficiency of the Ni-ZnO nanostructures with varied morphologies, three other nanostructures with flower-like, rod-like and wood-like morphologies, as shown in Fig. 9, were also considered.

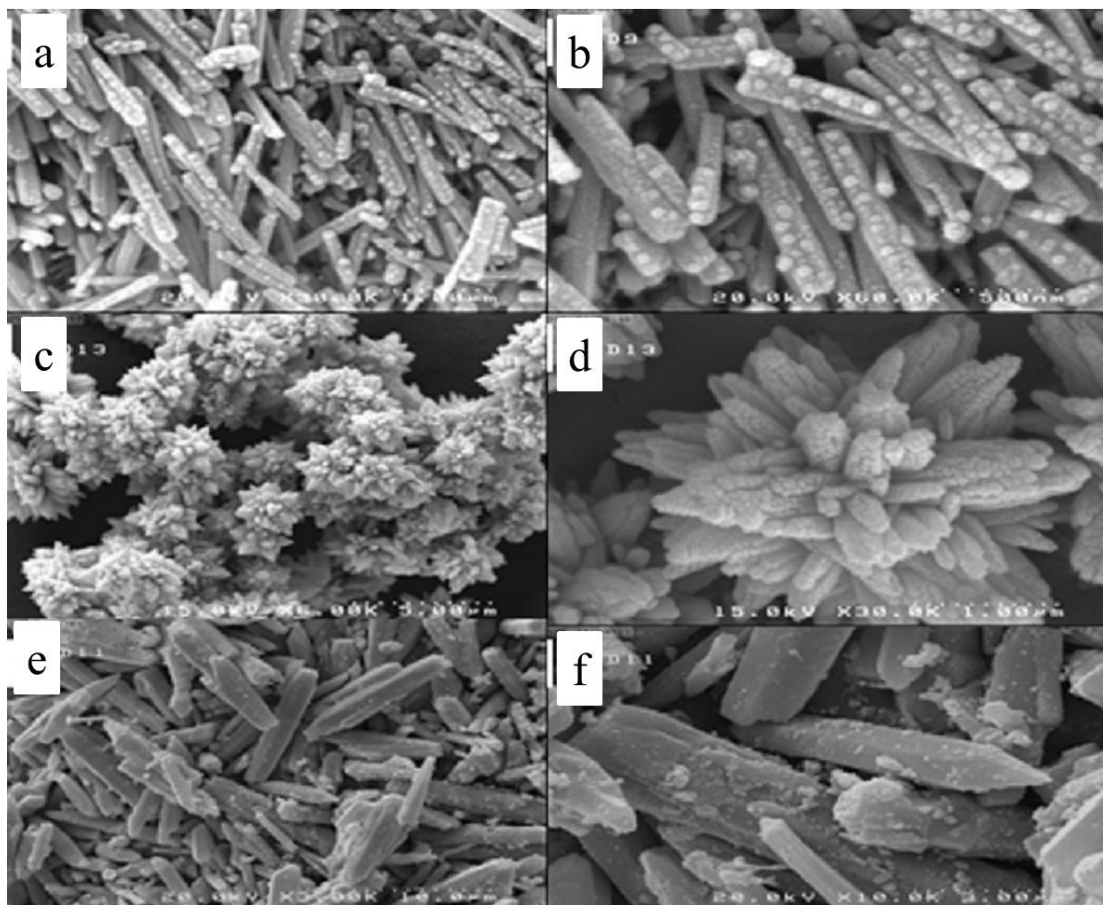


Fig. 9. SEM images of the 3-Ni-ZnO nanostructures synthesized via solvothermal (a, b), microwave (c, d), and sol-gel (e, f).

The photocatalytic properties of these nanostructures were then compared with that of the Ni-ZnO hollow spheres. Based on the results, in the visible light region, these morphologies are not efficient even when the reaction time is lengthened for 120 minutes. As Fig. 10 shows, under visible irradiation, the rod-like, flower-like, and wood-like morphologies have an efficiency of 79%, 69%, and 55% after 120 min from the start of the reaction, respectively.

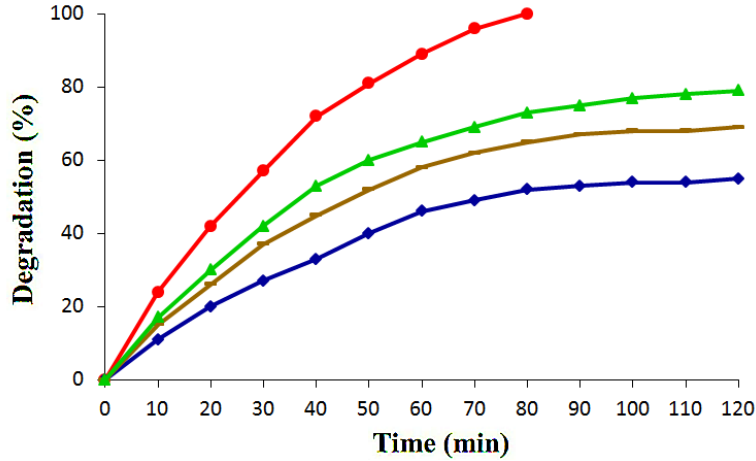
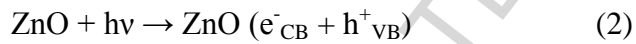
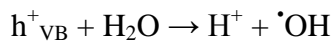
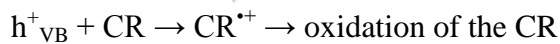


Fig. 10. Photocatalytic efficiency of the 3-Ni-ZnO nanostructures with different morphologies [wood like (blue), flower like (brown), rod like (green), and hollow sphere (red)] for CR dye degradation under visible light.

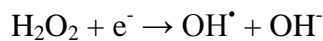
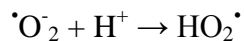
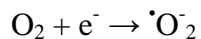
The CR dye is photo-catalytically removed under the following procedure. After the UV light irradiation ($\lambda = 598$ nm) of the Ni-doped ZnO, the electron-hole pairs are obtained from the excitation of a valence band electron to the band of conduction [37]. This is shown in Eq. (2):



After that, both the electron and the hole are able to react with the electron acceptors (e.g., O_2) and the electron donors (e.g., H_2O and OH^-) in a way that some very reactive radical species such as hydroxyl radicals ($E_0 = +3.06$ V) can be produced [37].



On the whole, because of metallic ion doping in a semiconductor, a shifting in Fermi level toward more negative potentials occurs and the interfacial charge transfer procedure becomes more efficient [38]. Consequently, in Ni/ZnO structure, the electron transfer from ZnO band of conduction to the novel Fermi level (E_f) takes place [39]. Accordingly, the CR dye photodegradation is improved by the hollow spheres of Ni-ZnO since these hollow spheres yield a greater number of hydroxyl radicals than the pure form of ZnO. Moreover, in the novel Fermi level, the absorbed O_2 can readily entrap the photo-generated electrons [40]. As such, superoxide radicals are synthesized and subsequently HO_2 molecules are made in the presence of water [40, 41]. After the hydroxyl radicals are produced, reduction of HO_2 to H_2O_2 happens. Note that the hydroxyl radicals are the main species causing the molecular dye degradation [40, 42].



Acknowledgements

This work was supported by the Tarbiat Modares University. The authors are grateful for the financial support.

4. Conclusion

In this work, pure ZnO and Ni-ZnO hollow spheres have been produced using a green chemical protocol. Based on the XRD and IR results, these hollow spheres are observed to be formed without any structural disorder. Furthermore, EDX results are indicative of the existence of Zn,

Ni and O elements in the synthesized Ni-ZnO hollow spheres. It has also been found that the Ni-ZnO hollow spheres have a better photocatalytic performance than the single ZnO for the CR dye degradation. Among the x-Ni-ZnO hollow spheres, the most photocatalytic activity is related to the 3-Ni-ZnO hollow spheres. Moreover, it has been found that our synthesized Ni-ZnO hollow spheres have superior photocatalytic characteristics, compared to other morphologies.

ACCEPTED MANUSCRIPT

References

- [1] W. Wang, M. O. Tadé, Z. Shao, Research progress of perovskite materials in photocatalysis- and photovoltaics-related energy conversion and environmental treatment, *Chem. Soc. Rev.* 44 (2015) 5371–5408.
- [2] S. Chaudhary, Y. Kaur, A. Umar, G. R. Chaudhary, 1-butyl-3-methylimidazolium tetrafluoroborate functionalized ZnO nanoparticles for removal of toxic organic dyes, *J. Mol. Liq.* 220 (2016) 1013–1021.
- [3] Q. Yang, H. Song, Y. Li, Z. Pan, M. Dong, F. Chen, Z. Chen, Flower-like core-shell Fe₃O₄@MnO₂ microspheres: Synthesis and selective removal of Congo red dye from aqueous solution, *J. Mol. Liq.* 234 (2017) 18–23.
- [4] R. Asahi, T. Morikawa, H. Irie, T. Ohwaki, nitrogen-doped titanium dioxide as visible-light-sensitive photocatalyst: designs, developments, and prospects, *Chem. Rev.* 114 (2014) 9824–9852.
- [5] M. Tobajas, C. Belver, J.J. Rodriguez, Degradation of emerging pollutants in water under solar irradiation using novel TiO₂-ZnO/clay nanoarchitectures, *Chem. Eng. J.* 309 (2017) 596–606.
- [6] R. Saravanan, V. K. Gupta, V. Narayanan, A. Stephen, Comparative study on photocatalytic activity of ZnO prepared by different methods, *J. Mol. Liq.* 181 (2013) 133–141.
- [7] S. Rajendran, M. M. Khan, F. Gracia, J. Qin, V. K. Gupta, S. Arumainathan, Ce³⁺-ion-induced visible-light photocatalytic degradation and electrochemical activity of ZnO/CeO₂ nanocomposite, *Scientific Reports* 6 (2016) 31641.

- [8] R. Abazari, A. R. Mahjoub, S. Sanati, A facile and efficient preparation of anatase titania nanoparticles in micelle nanoreactors: morphology, structure, and their high photocatalytic activity under UV light illumination, *RSC Adv.* 4 (2014) 56406–56414.
- [9] J. Schneider, M. Matsuoka, M. Takeuchi, J. Zhang, Y. Horiuchi, M. Anpo, D. W. Bahnemann, Understanding TiO₂ Photocatalysis: Mechanisms and Materials, *Chem. Rev.* 114 (2014) 9919–9986.
- [10] R. Saravanan, V. K. Gupta, E. Mosquera, F. Gracia, Preparation and characterization of V₂O₅/ZnO nanocomposite system for photocatalytic application, *J. Mol. Liq.* 198 (2014) 409–412.
- [11] R. Saravanan, F. Gracia, M. M. Khan, V. Poornima, V. K. Gupta, V. Narayanan, A. Stephen, ZnO/CdO nanocomposites for textile effluent degradation and electrochemical detection, *J. Mol. Liq.* 209 (2015) 374–380.
- [12] X. Pang, W. Chang, C. Chen, H. Ji, W. Ma, J. Zhao, Determining the TiO₂-Photocatalytic Aryl-Ring-Opening Mechanism in Aqueous Solution Using Oxygen-18 Labeled O₂ and H₂O, *J. Am. Chem. Soc.* 136 (2014) 8714–8721.
- [13] R. Saravanan, N. Karthikeyan, V. K. Gupta, E. Thirumal, P. Thangadurai, V. Narayanan, A. Stephen, ZnO/Ag nanocomposite: An efficient catalyst for degradation studies of textile effluents under visible light, *Materials Science and Engineering C* 33 (2013) 2235–2244.
- [14] R. Saravanan, M. M. Khan, V. K. Gupta, E. Mosquera, F. Gracia, V. Narayanan, A. Stephen, ZnO/Ag/CdO nanocomposite for visible light-induced photocatalytic degradation of industrial textile effluents, *Journal of Colloid and Interface Science* 452 (2015) 126–133.
- [15] R. Saravanan, M. M. Khan, V. K. Gupta, E. Mosquera, F. Gracia, V. Narayanan, A. Stephen, ZnO/Ag/Mn₂O₃ nanocomposite for visible lightinduced industrial textile effluent

degradation, uric acid and ascorbic acid sensing and antimicrobial activity, *RSC Adv.* 5 (2015) 34645–34651.

[16] R. Saravanan, H. Shankar, T. Prakash, V. Narayanan, A. Stephen, ZnO/CdO composite nanorods for photocatalytic degradation of methylene blue under visible light, *Materials Chemistry and Physics* 125 (2011) 277–280.

[17] R. Kumar, S. Anandan, K. Hembram, T. N. Rao, Efficient ZnO-Based Visible-Light-Driven Photocatalyst for Antibacterial Applications, *ACS Appl. Mater. Interfaces* 6 (2014) 13138–13148.

[18] D. Hong, W. Zang, X. Guo, Y. Fu, H. He, J. Sun, L.-L. Xing, B. Liu, X. Xue, Article High Piezo-Photocatalytic Efficiency of CuS/ZnO Nanowires CoUsing Solar and Mechanical Energy for Degrading Organic Dye, *ACS Appl. Mater. Interfaces*, 8 (2016) 21302–21314.

[19] R. Saravanan, E. Sacari, F. Gracia, M. M. Khan, E. Mosquera, V. K. Gupta, Conducting PANI stimulated ZnO system for visible light photocatalytic degradation of coloured dyes, *J. Mol. Liq.* 221 (2016) 1029–1033.

[20] F. G. Shahna, A. Bahrami, I. Alimohammadi, R. Yarahmadi, B. Jaleh, M. Gandomi, H. Ebrahimi, K. Ad-D. Abedi, Chlorobenzene degeradation by non-thermal plasma combined with EG-TiO₂/ZnO as a photocatalyst: Effect of photocatalyst on CO₂ selectivity and byproducts reduction, *J. Hazard. Mater.* 324 (2017) 544–553.

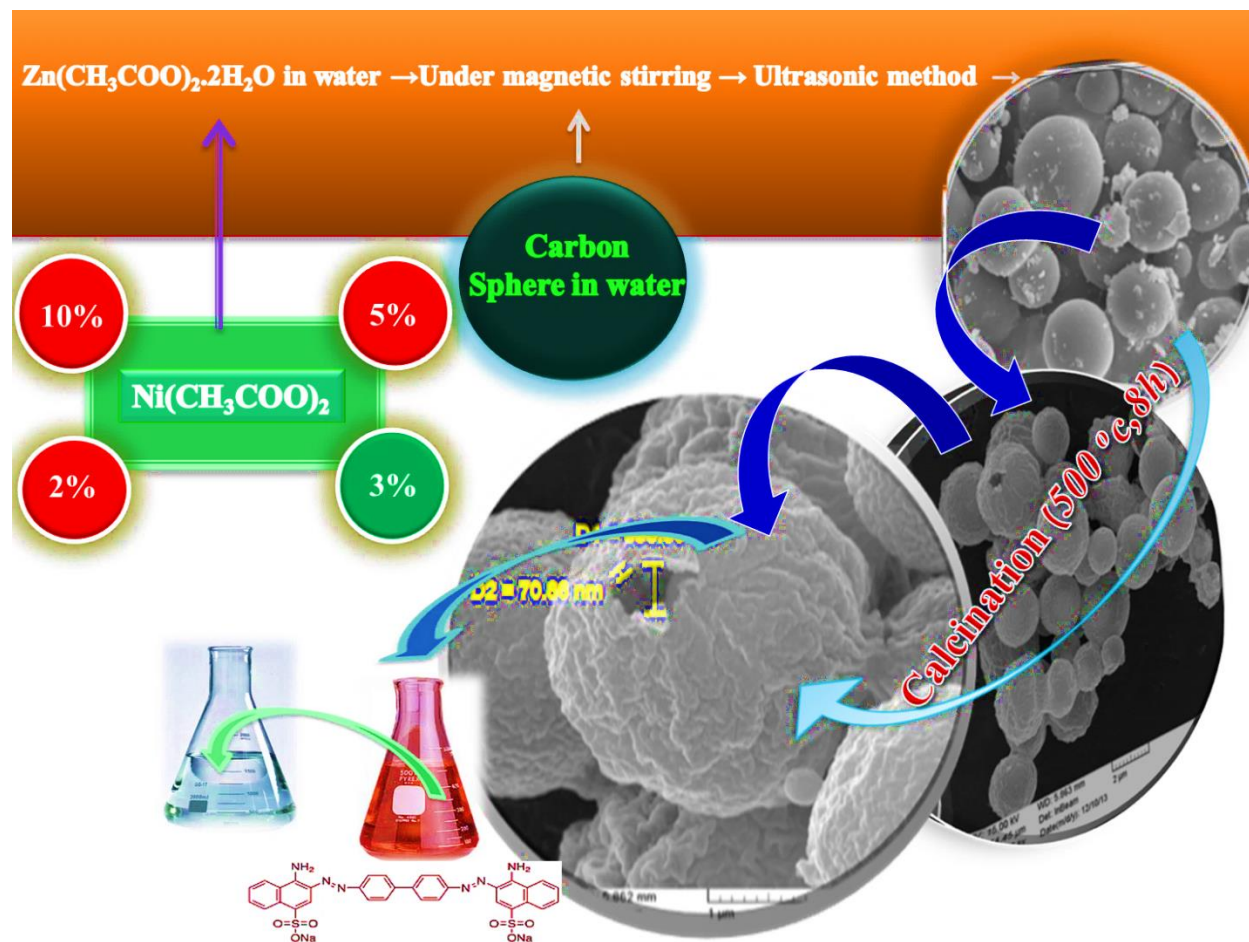
[21] C. H. Joseph, G. M. Sardi, S.S. Tuca, G. Gramse, A. Lucibello, E. Proietti, F. Kienberger, R. Marcelli, Scanning Microwave Microscopy Technique for Nanoscale Characterization of Magnetic Materials, *J. Magn. Magn. Mater.* 420 (2016) 62–69.

- [22] Z. Liu, M. Zhang, X. Xu, L. Bu, W. Zhang, W. Li, Z. Zhao, M. Wang, Y.-B. Chenga, H. He, p-Type mesoscopic NiO as an active interfacial layer for carbon counter electrode based perovskite solar cells, *Dalton Trans.* 44 (2015) 3967–3973.
- [23] Z. Rena, Z. Wu, W. Song, W. Xiao, Y. Guo, J. Ding, S. L. Suib, P.-Xi. Gao, Low temperature propane oxidation over Co_3O_4 based nano-array catalysts: Ni dopant effect, reaction mechanism and structural stability, *Appl. Catal., B* 180 (2016) 150–160.
- [24] Y. Fu, L. Sun, H. Yang, L. Xu, F. Zhang, W. Zhu, Visible-light-induced aerobic photocatalytic oxidation of aromatic alcohols to aldehydes over Ni-doped $\text{NH}_2\text{-MIL-125(Ti)}$, *Appl. Catal., B* 187 (2016) 212–217.
- [25] S. G. Ghugal, R. R. Mahalik, P. S. Charde, S. S. Umare, S. B. Kokane, V. Sudarsan, R. Sasikal, Photocatalytic properties of mesoporous alumina containing Ni doped CdS nanostructures, *Microporous Mesoporous Mater.* 242 (2017) 284–293.
- [26] R. Abazari, A. R. Mahjoub, Potential Applications of Magnetic $\beta\text{-AgVO}_3/\text{ZnFe}_2\text{O}_4$ Nanocomposites in Dyes, Photocatalytic Degradation, and Catalytic Thermal Decomposition of Ammonium Perchlorate, *Ind. Eng. Chem. Res.* 56 (2017) 623–634.
- [27] R. Abazari, A. R. Mahjoub, S. Sanati, Magnetically recoverable $\text{Fe}_3\text{O}_4\text{-ZnO/AOT}$ nanocomposites: Synthesis of a core–shell structure via a novel and mild route for photocatalytic degradation of toxic dyes, *J. Mol. Liq.* 223 (2016) 1133–1142.
- [28] R. Abazari, S. Sanati, Room temperature synthesis of tungsten (VI) tri-oxide nanoparticles with one-pot multi-component reaction in emulsion nanoreactors stabilized by aerosol-OT, *Mater. Lett.* 107 (2013) 329–332.

- [29] C. Liu, L. Zhao, B. Wang, P. Sun, Q. Wang, Y. Gao, X. Liang, T. Zhang, G. Lu, Acetone gas sensor based on NiO/ZnO hollow spheres: Fast response and recovery, and low (ppb) detection limit, *J. Colloid Interface Sci.* 495 (2017) 207–215.
- [30] S. M. Mousavi, A. R. Mahjoub, R. Abazari, Green synthesis of ZnO hollow sphere nanostructures by facile route at room temperature with efficient photocatalytic dye degradation, *RSC Adv.* 5 (2015) 107378–107388.
- [31] H. M. Abdelaal, B. Harbrecht, Fabrication of hollow spheres of metal oxide using fructose-derived carbonaceous spheres as sacrificial templates, *C. R. Chimie* 18 (2015) 379–384.
- [32] S. G. Hosseini, R. Abazari, A facile one-step route for production of CuO, NiO, and CuO–NiO nanoparticles and comparison of their catalytic activity for ammonium perchlorate decomposition, *RSC Adv.* 5 (2015) 96777–96784.
- [33] F. Fazlali, A. R. Mahjoub and R. Abazari, A new route for synthesis of spherical NiO nanoparticles via emulsion nano-reactors with Enhanced Photocatalytic Activity, *Solid State Sci.* 48 (2015) 263–269.
- [34] E. Safaralizadeh, S. Janitabar Darzi, A. R. Mahjoub, R. Abazari, Visible light-induced degradation of phenolic compounds by Sudan black dye sensitized TiO₂ nanoparticles as an advanced photocatalytic material, *Res. Chem. Intermed.* 43 (2017) 1197–1209.
- [35] B. Wang, G. Wang, X. Cheng, H. Wang, Synthesis and electrochemical investigation of core-shell ultrathin NiO nanosheets grown on hollow carbon microspheres composite for high performance lithium and sodium ion batteries, *Chem. Eng. J.* 306 (2016) 1193–1202.
- [36] S. C. Das, R. J. Green, J. Podder, T. Z. Regier, G. S. Chang, A. Moewes, Band gap tuning in ZnO through Ni doping via spray pyrolysis, *J. Phys. Chem. C* 117 (2013) 12745–12753.

- [37] M. Qamar, M. Muneer, A comparative photocatalytic activity of titanium dioxide and zinc oxide by investigating the degradation of vanillin, *Desalination* 249 (2009) 535–540.
- [38] V. Subramanian, E. E. Wolf, P. V. Kamat, Catalysis with TiO₂/Gold nanocomposites. Effect of metal particle size on the fermi level equilibration, *J. Am. Chem. Soc.* 126 (2004) 4943–4950.
- [39] R. Georgekutty, M. K. Seery, S. C. Pillai, A highly efficient Ag-ZnO photocatalyst: synthesis, properties, and mechanism, *J. Phys. Chem. C* 112 (2008) 13563–13570.
- [40] S. Senapati, S. K. Srivastava, S. B. Singh, Synthesis, characterization and photocatalytic activity of magnetically separable hexagonal Ni/ZnO nanostructure, *Nanoscale* 4 (2012) 6604–6612.
- [41] V. K. Gupta, R. Saravanan, S. Agarwal, F. Gracia, M. Mansoob Khan, J. Qin, R. V. Mangalaraja, Degradation of azo dyes under different wavelengths of UV light with chitosan-SnO₂ nanocomposites, *J. Mol. Liq.* 232 (2017) 423–430.
- [42] L. Gnanasekaran, R. Hemamalini, R. Saravanan, K. Ravichandran, F. Gracia, V. K. Gupta, Intermediate state created by dopant ions (Mn, Co and Zr) into TiO₂ nanoparticles for degradation of dyes under visible light, *J. Mol. Liq.* 223 (2016) 652–659.

Graphical Abstract:



Research Highlights:

- Nanostructural Ni-doped ZnO hollow spheres were prepared via a facile chemical route.
- These hollow spheres have been used for first time for the CR dye degradation.
- X-Ni-doped ZnO hollow spheres showed high visible light photocatalytic activity for CR dye degradation.
- Degradation efficiency for 3-Ni-doped ZnO hollow sphere was over 99%.
- Improved electron–hole separation due to addition of Ni²⁺ ions for CR dye degradation.